substance: La_2S_3
property: crystal structure, physical properties

α-La_2S_3

crystal structure	orthorhombic (D_{2h}^{16} – Pnma)			
lattice parameters				
a	7.584 Å			68S
	7.587(7) Å			81G
b	15.860 Å			68S
	15.863(4) Å			81G
c	4.144 Å			68S
	4.149(2) Å			81G
melting point				
T_m	1950°C			81G
Debye temperature				
Θ_D	317(1) K			81G

heat capacity: Fig. 1

β-La_2S_3

crystal structure	tetragonal (D_{4h}^{20} – $I4_1/acd$)			
a = *b*	15.62 Å			73B
	15.65(4) Å			81G
c	20.62 Å			73B
	20.64(6) A			81G
energy gap				
E_g	2.58 eV	direct	optical determination	80L
	2.6 eV	direct	fundamental absorption edge	81S
	1.38 eV		indirect or impurity tail	80L
resistivity				
ρ	$2 \cdot 10^{12}...4 \cdot 10^{14}$ Ω cm			82A

Figures and further references for β-La_2S_3:

phase transition β → γ at 1300°C

heat capacity: Fig. 2; for heat capacity, enthalpy and entropy, see also [69P]

optical spectra for Nd-doped crystals: Figs. 3, 4; optical spectra for Nd, Ce-codoped crystals: Figs. 5, 6, 7

photoconductivity of a Ce-doped crystal: Fig. 8

photoluminescence, cathodoluminescence of a Ce-doped crystal: Figs. 9, 10

γ-La_2S_3

crystal structure cubic (Th_3P_4-defect structure, $T_d^6 - I\bar{4}3d$)

lattice parameters

a	8.723 Å			85Z
	8.726(1) Å			78K
	8.731 Å			60P
	8.7253(8) Å			76K
	8.725 Å			81K
	8.69 Å			80K

melting point

T_m	2080°C			60P
	1980(30)°C			76K, 81K
	2100°C			80K

density

d	4.93 g cm^{-3}			60P

linear thermal expansion coefficient

α	$9.9 \cdot 10^{-6}$ K^{-1}			66D

energy gap and other energy parameters

E_g	2.76 ± 0.1 eV		optical energy gap	85Z
	2.8 ± 0.25 eV		thermodynamic	85Z
	1.9 eV		X-ray spectra	83S
	2.9 eV		optical gap	80K
	2.4 eV	*T* = 148 K	optical gap	82B, 81B
	2.8(1) eV		optical gap	79Z
dE_g/dT	$4.9 \cdot 10^{-4}$ eV/K	*T* = 250 K...350 K		79Z

E_b	4.8 eV	S 3p-level	MgKα XPS, Fig. 24 (E_b rel. to E_F)	91K
	13.6 eV	S 3s-level	MgKα XPS, Fig. 24	
	18.9 eV	La $5p_{3/2}$-level	MgKα XPS, Fig. 24	
	20.9 eV	La $5p_{1/2}$-level	MgKα XPS, Fig. 24	
	36 eV	La 5s-level	MgKα XPS, Fig. 25	
	103 eV	La $4d_{5/2}$-level	MgKα XPS, Fig. 25	
	104 eV	La $4d_{3/2}$-level	MgKα XPS, Fig. 25	
	197 eV	La $4p_{3/2}$-level	MgKα XPS	
	209 eV	La $4p_{1/2}$-level	MgKα XPS	
	834 eV	La $3d_{5/2}$-level	AlKα XPS, Fig. 26	
	851 eV	La $3d_{3/2}$-level	AlKα XPS, Fig. 26	
E	5.9 eV	S 3p-E_F	ELS, Fig. 27	91K
	11.1 eV	S 3p-cond. band, surface plasmon	ELS, Fig. 27	
	16.1 eV	bulk plasmon	ELS, Fig. 27	
	20.8 eV	La 5p-E_F	ELS, Fig. 27	
	27.5 eV	La 5p-5d	ELS, Fig. 27	
	≈ 37 eV	La 5s-E_F	ELS, Fig. 27	
	118 eV	La 4d-4f	ELS, Fig. 28	
			reflectivity: Fig. 29	

thermal conductivity

κ	$2.3 \cdot 10^{-2}$ W cm^{-1} K^{-1}		72G	

Debye temperature

Θ_D	320 K			72S
	285 K			81G

phonon wavenumbers

$(\nu/c)_{TO}$	195 cm^{-1}		(ν/c) from Raman spectrum	79A
	230 cm^{-1}			
$(\nu/c)_{LO}$	301 cm^{-1}			

dielectric constants

$\varepsilon(0)$	17.2			79A
$\varepsilon(\infty)$	7.0			79A, 79Z

refractive index

n	2.6	λ = 1...15 µm		80K
	2.8	λ = 0.55 µm		

electrical conductivity

σ	10^{-10} Ω^{-1} cm^{-1}			80K
	10^{-9}...10^{-10} Ω^{-1} cm^{-1}			79Z
	$0.7 \cdot 10^{-12}$ Ω^{-1} cm^{-1}			81B
	10^{-12} Ω^{-1} cm^{-1}	T = 145 K		82B

Further figures and references for γ-La_2S_3:

phase diagram: Fig. 11

coordination polyhedra: Fig. 12

Raman spectrum: Figs. 13, 14

absorption and transmission spectra: Figs. 14, 15, 16

real and imaginary part of the **dielectric constant**: Fig. 17

reflectivity spectrum: Fig. 18

luminescence and absorption of Nd-doped crystals: Figs. 19...23

References:

60P Picon, M., Domange, L., Flahaut, J., Guittard, M., Patrie, M.: Bull. Soc. Chim. Fr. 2 (1960) 221.
66D Dudnik, E. M., Lashkarev, G. V., Paderno, Y. B., Obolonchik, V. A.: Inorg. Mater. 2 (1966) 833.
66H Holtzberg, F., Methfessel, S.: J. Appl. Phys. 37 (1966) 1433.
67B Berkooz, O., Malamud, M., Shtrikman, S.: Solid State Commun. 6 (1967) 185.
68S Sleight, A. W., Prewitt, C. T.: Inorg. Chem. 7 (1968) 2282.
69P Pankov, I. E., Nogteva, V. V., Yarembash, E. I.: Russ. J. Phys. Chem. 43 (1969) 1316.
72G Goryachev, Yu. M., Kutsenok, T. G.: High Temp. High Press. 4 (1972) 663.
72S Smirnov, I. A.: Phys. Status Solidi (a) 14 (1972) 363.
73B Besancon, P.: J. Solid State Chem. 7 (1973) 232.
76K Kamarzin, A. A., Sokolov, V. V., Mironov, K. E., Maloviikii, N, Vasileva, I. G.: Mater. Res. Bull. 11 (1976) 695.
78K Konstantinov, V. L., Skornyakov, G. P., Kamarzin, A. A., Sokolov, V. V.: Inorg. Mater. 14 (1978) 659.
79A Arkatova, T. G., Zhuze, V. P., Karin, M. G., Kamarzin, A. A., Kukharskii, A. A., Mikhailov, B. A., Shelykh, A. I.: Sov. Phys. Solid State 21 (1979) 1979.
79Z Zhuze, V. P., Kamarzin, A. A., Karin, M. G., Sidorin, K. K., Shelykh, A. I.: Sov, Phys. Solid State 21 (1979) 1968.
80K Kaminskii, A. A., Sarkisov, C. E., Chan Niok, Denisenko, G. A., Kamarzin, A. A., Sokolov, V. V., Klypin, V. V., Maloviikii, Yu. N.: Izv. Akad. Nauk SSSR, Neorg. Mater. 16 (1980) 1333.
80L Leiss, M.: J. Phys. C 13 (1980) 151.
81B Batirov, T. M., Fridkin, V. M., Kamarzin, A. A., Malovitskii, Y. I., Verkhovskaya, K. A.: Phys. Status Solidi (a) 65 (1981) K163.
81G Gschneidner, K. A., Beaudry, B. J., Takeshita, T., Eucker, S. S., Taher, S. M. A., Ho, J. C., Gruber, J. B.: Phys. Rev. B 24 (1981) 7187.
81K Kamarzin, A. A., Mironov, K. E., Sokolov, V. V., Malovitskii, Y. N., Vasil'yeva, I. G.: J. Cryst. Growth 52 (1981) 619.
81S Scharmer, E. G., Leiß, M., Huber, G.: J. Lumin. 24/25 (1981) 751.
82A Astalleva, L. V., Skornyakov, G. P., Kamarzin, A. A., Malovitskii, Y. N.: Sov. Phys. Solid State 24 (1982) 367.
82B Batirov, T. M., Verkhovskaya, K. A., Kamarzin, A. A., Malovitskii, Y. N., Lisoivan, V. I., Fridkin, V. M.: Sov. Phys. Solid State 24 (1982) 746.
82S Scharmer, E. G., Leiß, M., Huber, G.: J. Phys. C 15 (1982) 1071.
83B Balabanova, L.A., Zhuze, V.P., Ostroumova, E.G., Shul'man, S.G.: Sov. Phys. Solid State 25(6) (1983) 971.
83K1 Kamarzin, A. A., Mamedov, A. A., Smirnov, V. A., Sobol', A. A., Sokolov, V. V., Shcherbakov, I. A.: Sov. J. Quantum Electron. 13 (1983) 1027.
83K2 Kamarzin, A. A., Mamedov, A. A., Smirnov, V. A., Sokolov, V. V., Shcherbakov, I. A.: Sov. J. Quantum Electron. 13 (1983) 328.
83S Soldatov, A.V., Gusatinskii, A.N., Karin, M.G., Sidorin, K.K., Sadovskaya, O.A.: Inorg. Mater. 19 (1983) 951-954.
85Z Zhuze, V.P., Karin, M.G., Sidorin, K.K., Sokolov, V.V., Shelykh, A.I.: Sov. Phys. Solid State 27(12) (1985) 2205.
91K Kaciulis, S., Latisenka, A., Plesanovas A.: Surf. Sci. 251/252 (1991) 330.

Fig. 1.

α-La_2S_3. Temperature dependence of heat capacity [81G].

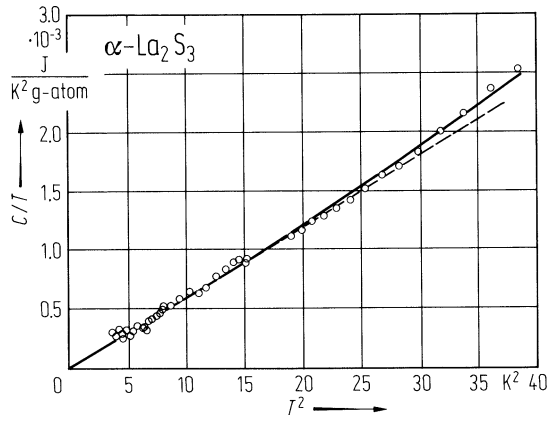

Fig. 2.

β-La_2S_3. Temperature dependence of heat capacity [81G].

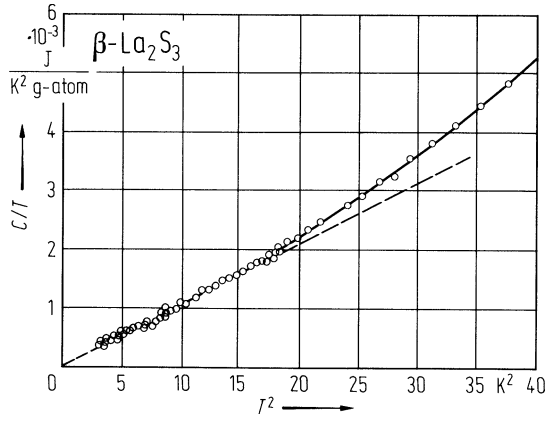

Fig. 3.

α-Gd_2S_3:Nd, β-La_2S_3:Nd, Y_2S_3:Nd. Absorbance *A* vs. wavelength [80L].

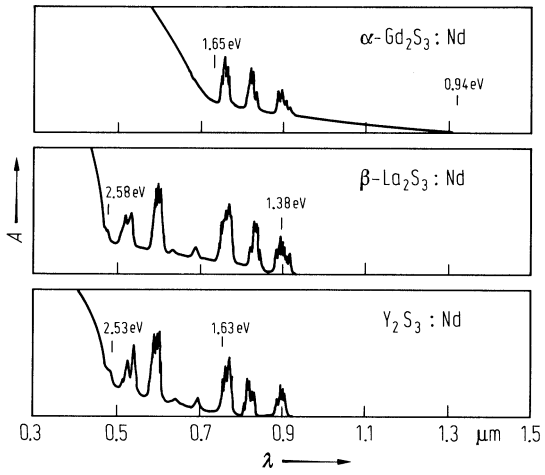

Fig. 4.

α-Gd_2S_3:Nd, β-La_2S_3:Nd, Y_2S_3:Nd. Photoluminescence intensity vs. wavelength for α-Gd_2S_3:Nd excited at 752.5 nm, β-La_2S_3:Nd and Y_2S_3:Nd excited at 600 nm [80L].

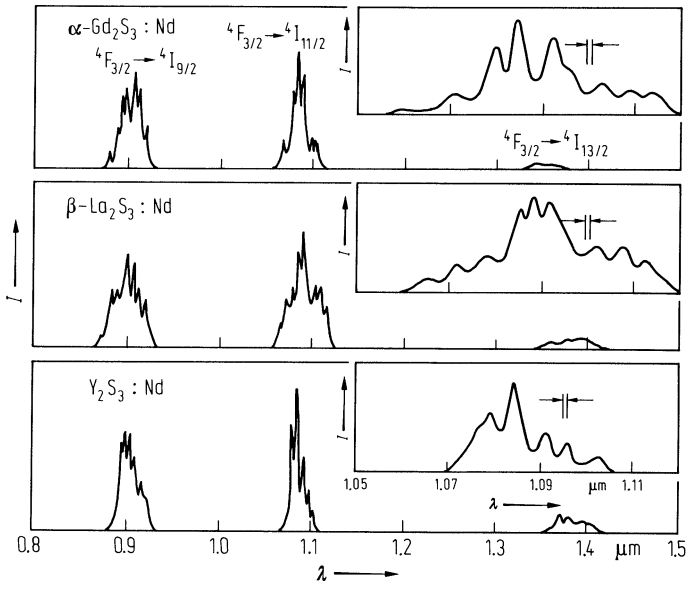

Fig. 5.

β-La_2S_3:Nd,Ce. Absorption spectrum (absorption coefficient vs. wavelength) of Nd(1%) and Ce(1%) co-doped crystals; unpolarized light [82S].

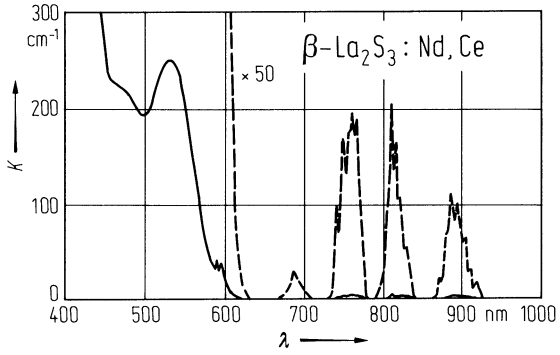

Fig. 6.

β-La_2S_3:Nd,Ce. Fluorescence spectra (fluorescence intensity vs. wavelength) of (A) Nd (10%), Ce(1%) and (B) Nd(1%), Ce (0.2%) codoped crystals [82S].

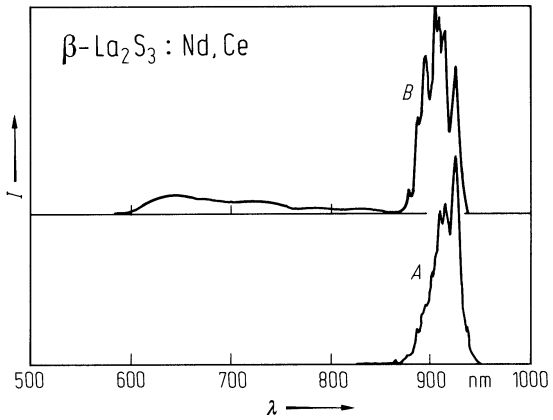

Fig. 7.

β-La_2S_3:Nd,Ce; β-La_2S_3:Nd. Excitation spectra of Nd^{3+} (fluorescence intensity vs. excitation wavelength) registered at λ = 900 nm for (A) Nd(1%) and (B) Nd(10%), Ce(1%) doped crystals. The codoped crystal (B) shows efficient energy transfer from band excitation to Nd^{3+} [82S]. *Q*: quantum efficiency of the transfer to Nd^{3+}.

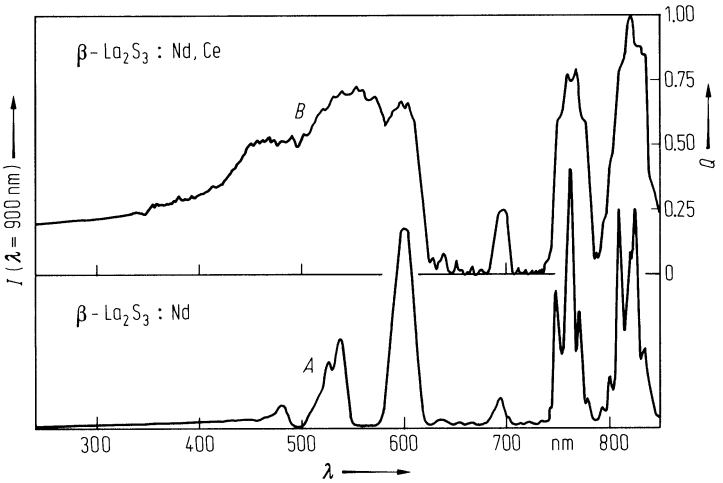

Fig. 8.

β-La_2S_3:Ce. Photoconductivity vs. wavelength for two crystals. (A): 1% Ce, (B): 0.05% Ce doping levels [82S].

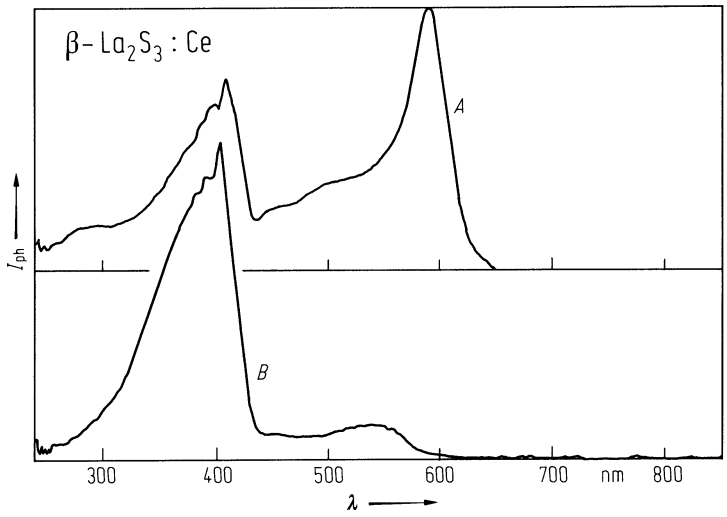

Fig. 9.

β-La_2S_3:Ce. Photoluminescence intensity vs. wavelength for two Ce doping levels [81S]. Excitation wavelength: 540 nm.

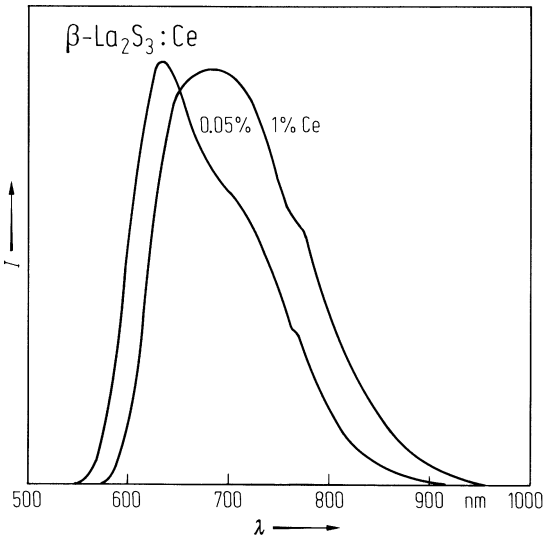

Fig. 10.

β-La_2S_3:Ce. Cathodoluminescence (intensity vs. wavelength) at two Ce doping levels for 20 kV electron beam excitation [81S].

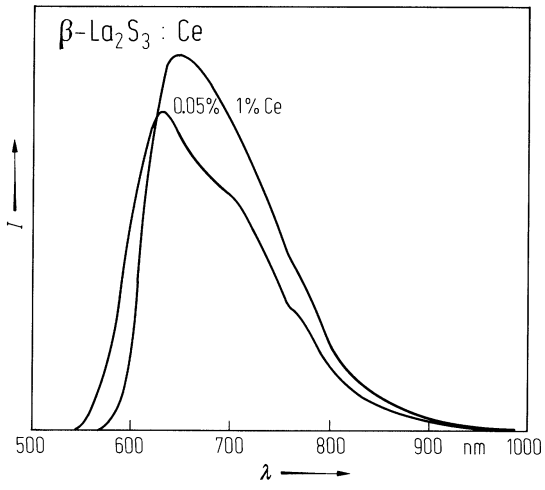

Fig. 11.

$LnS–Ln_2S_3$ system, Ln = La, Gd, Dy. Phase diagrams [81K].

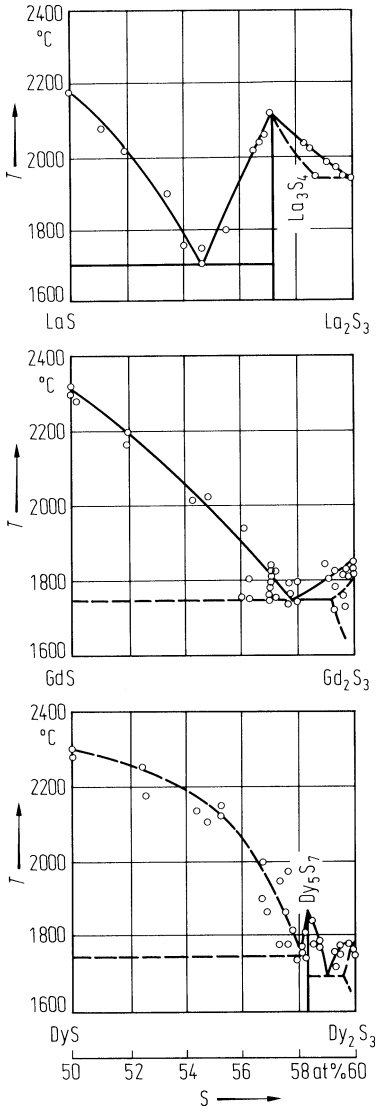

Fig. 12.

Th_3P_4-type compounds. The coordination polyhedra of the cations and the anions. Full circles: Th- atoms, other circles: P-atoms [66H].

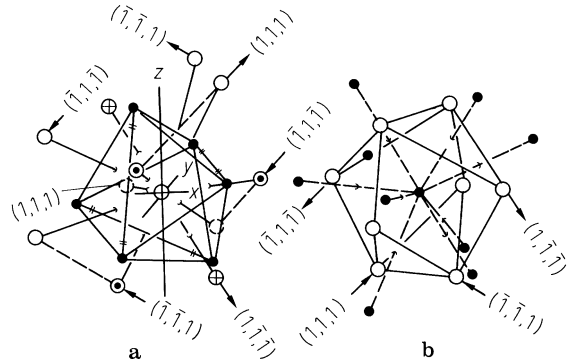

Fig. 13.

γ-La_2S_3. Raman intensity vs. Raman shift (in wavenumbers) [79A].

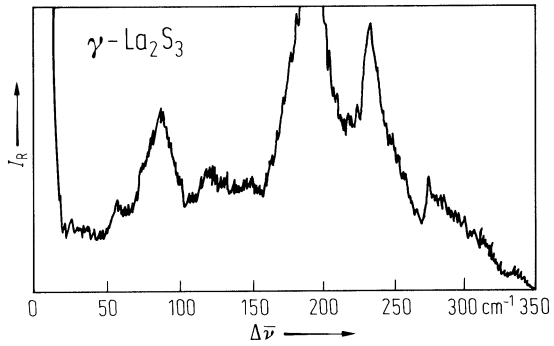

Fig. 14.

γ-La_2S_3, γ-Gd_2S_3. Infrared absorption and Raman intensity vs. wavenumber at 300 K [67B].

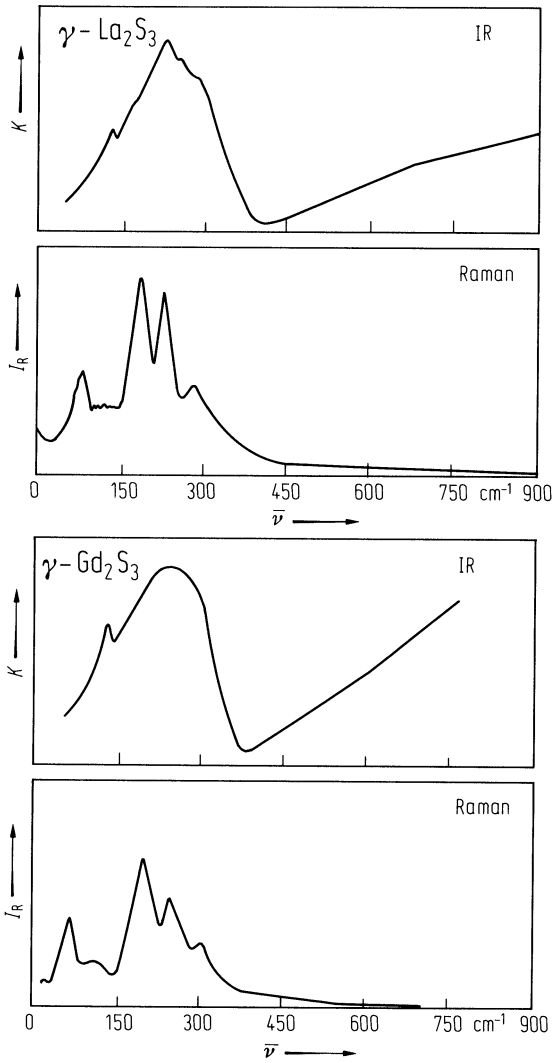

Fig. 15.

γ-La_2S_3, γ-Nd_2S_3, γ-Dy_2S_3. Absorption coefficient vs. photon energy [79Z].

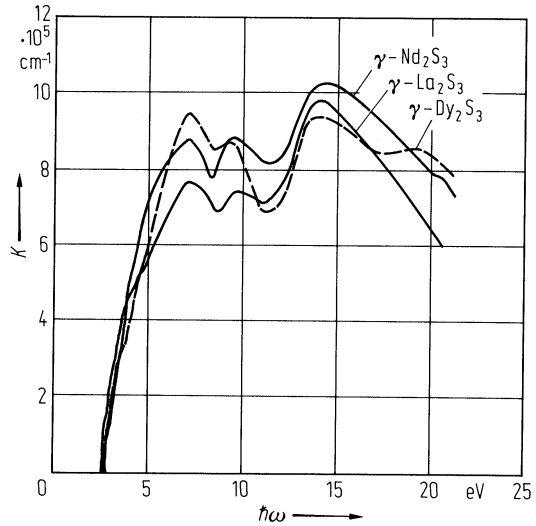

Fig. 16.

γ-La_2S_3. Transmission spectrum (transmission vs. wavelength) of a 315 μm thick single crystal platelet [81K].

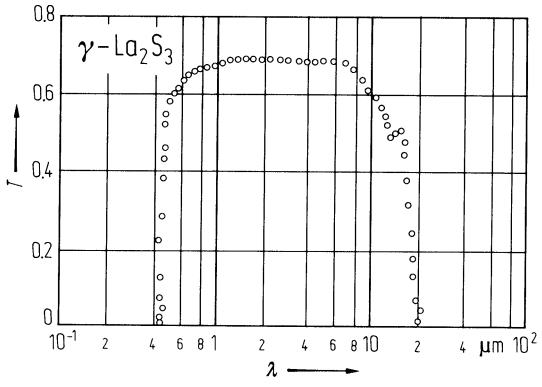

Fig. 17.

γ-La_2S_3. Real and imaginary parts of the dielectric constant and energy loss function vs. photon energy [79Z].

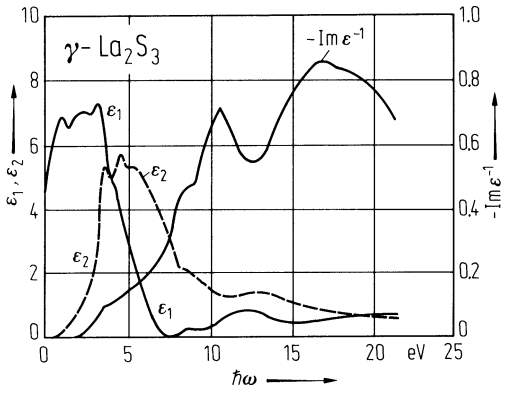

Fig. 18.

γ-La_2S_3, γ-Nd_2S_3, γ-Dy_2S_3. Reflectivity vs. wavenumber in the infrared range [79A].

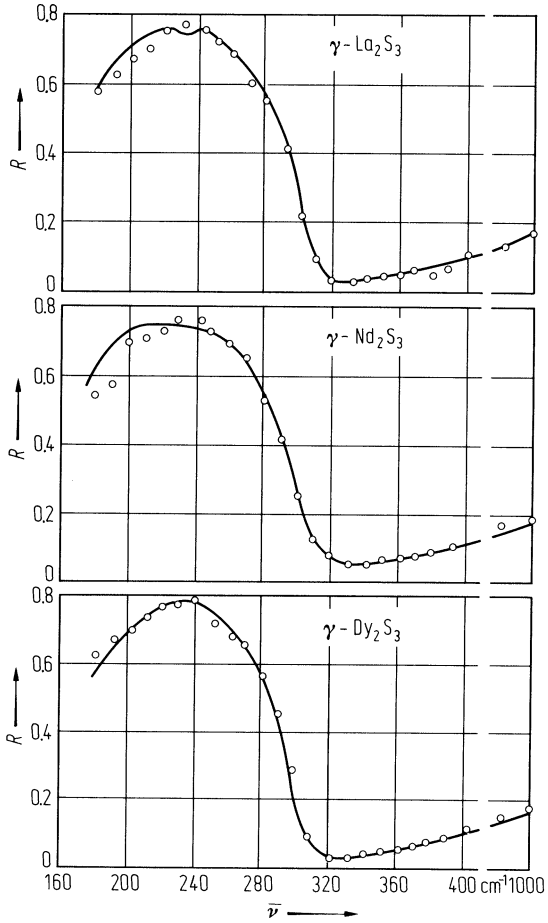

Fig. 19.

γ-La_2S_3:Nd. Absorption coefficient vs. wavelength at 300 K [80K]. Cf. Figs. 21, 22.

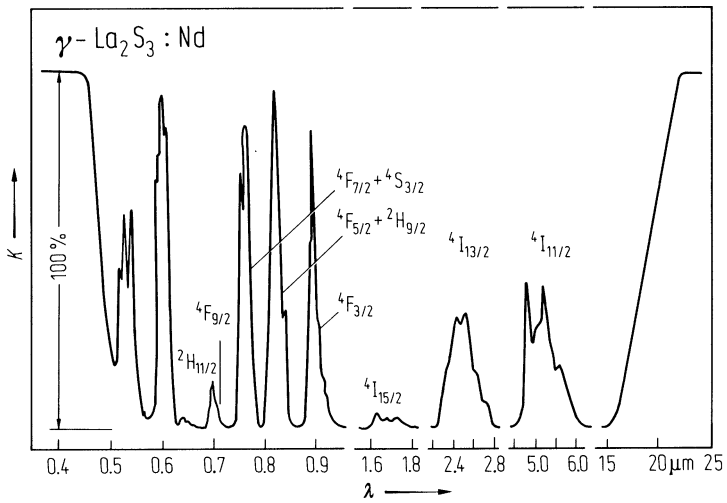

Fig. 20.

γ-La_2S_3:Nd (0.9%). Luminescence spectra (intensity vs. wavelength) with 530 nm excitation taken 1 μs (a), 5 μs (b), and 10 μs (c) after excitation [83K2].

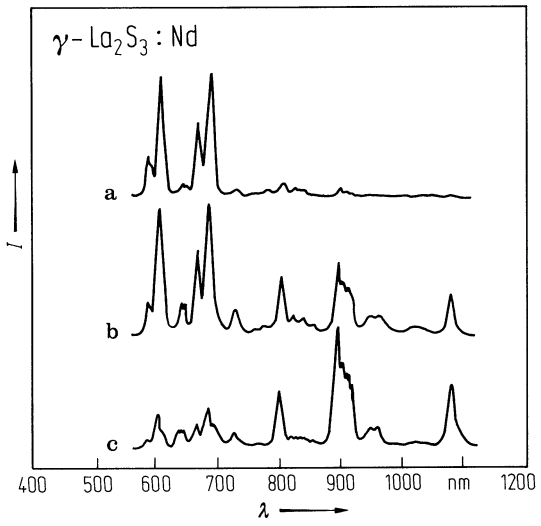

Fig. 21.

γ-La_2S_3:Nd (0.9%). Luminescence intensity (a) and absorption coefficient (b) vs. wavelength at 4.2 K [83K2].

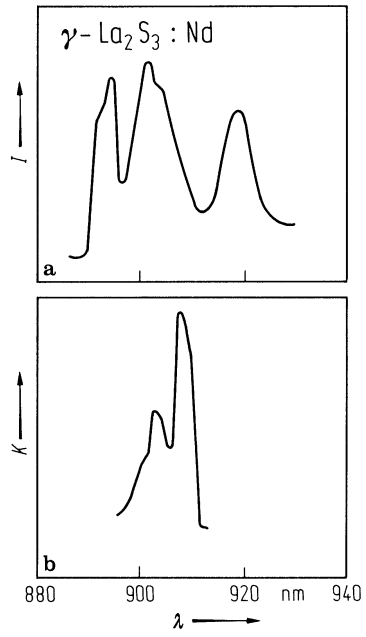

Fig. 22.

γ-La_2S_3 Nd (0.9%). Absorption coefficient vs. wavelength at 300 K (a) and 600 K (b) [83K1]. Cf Fig. 19.

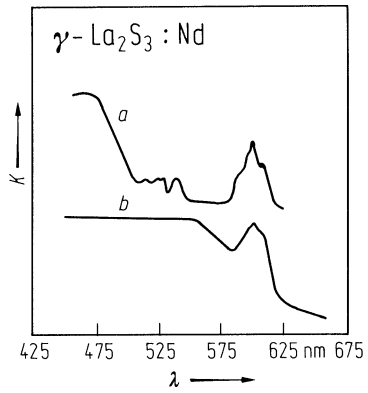

Fig. 23.

γ-($La_{1-x}Nd_x)_2S_3$. Temporal evolution of the $^4F_{3/2}$ neodymium population for x = 0.27 (*1*), 0.073 (*2*), 0.046 (*3*), 0.027 (*4*), 0.009 (*5*), and 0.003 (*6*) after a short pulse excitation at 530 nm (a) and 600 nm (b). (Normalized fluorescence intensity I/I_0 vs. time *t*) [83K2].

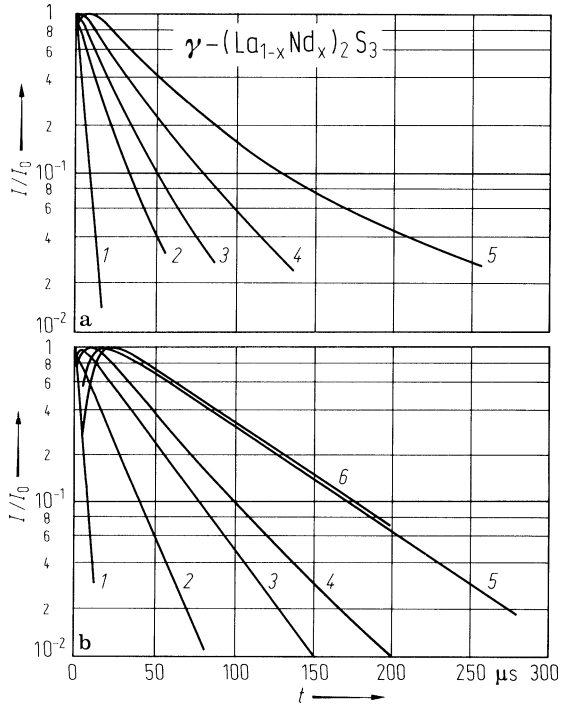

Fig. 24.

γ-Ln_2S_3. MgK_α X-ray photoelectron spectra of the rare-earth sesquisulfides (Ln = La, Ce, Nd, Sm, Gd, Dy) in the energy region below Fermi level down to Ln 5s core level [91K].

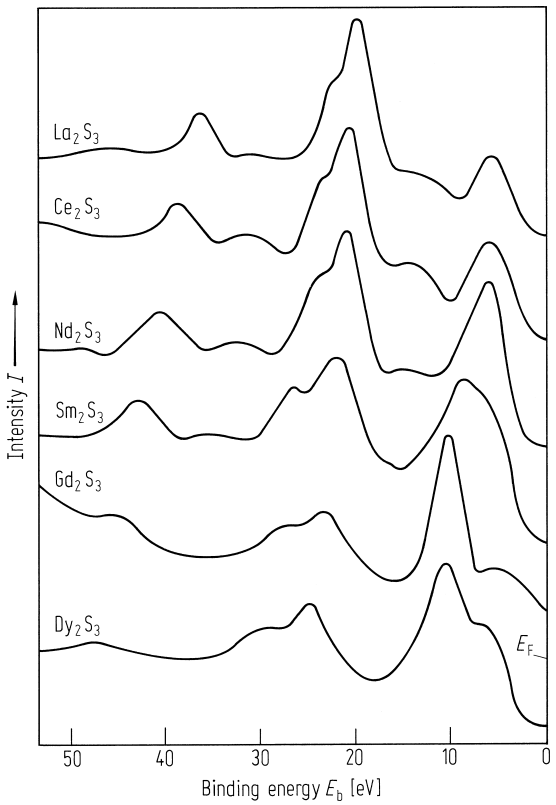

Fig. 25.

γ-Ln_2S_3. MgK_α X-ray photoelectron spectra of the rare-earth sesquisulfides (Ln = La, Ce, Nd, Sm, Gd, Dy) in the 4d core level region [91K]. E_b relative to E_F.

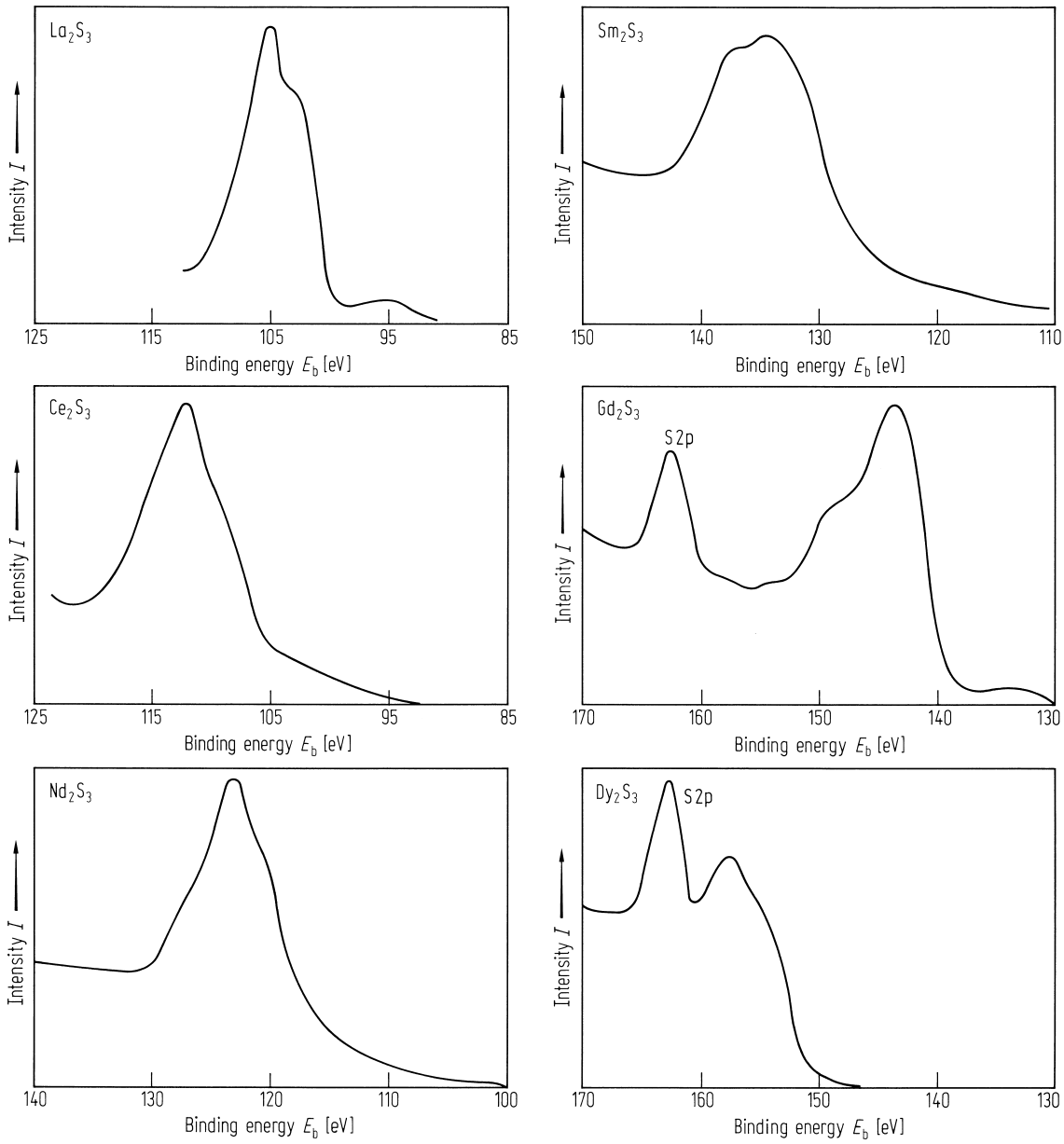

Fig. 26.

γ-Ln_2S_3. AlK_α X-ray photoelectron spectra of the rare-earth sesquisulfides (Ln = La, Nd, Sm, Gd) in the 3d core level region [91K]. The trivalence of Sm is testified by the value of the Sm 3d doublet line spin-orbit splitting (= 27.6 eV). E_b relative to E_F.

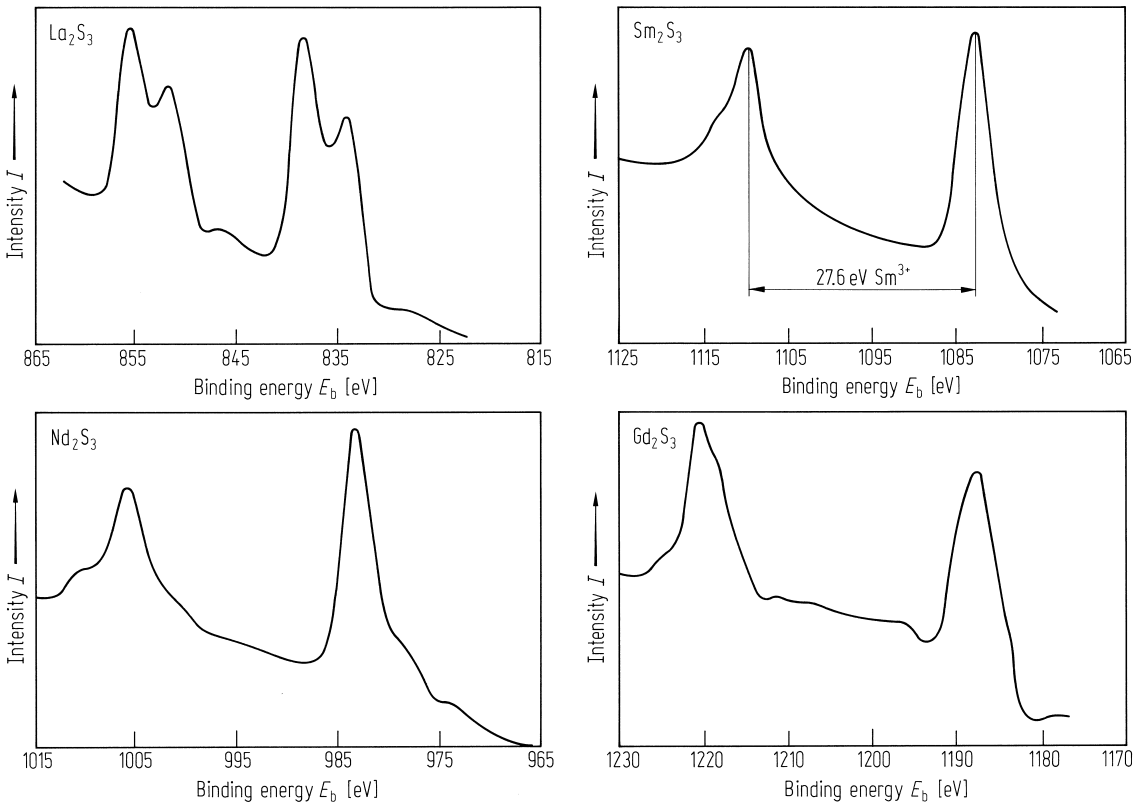

Fig. 27.

γ-Ln_2S_3. Electron loss spectra of the rare-earth sesquisulfides (Ln = La, Ce, Nd, Sm, Gd, Dy) for primary electron beam energy E_p = 750 eV. All the peaks, revealed from the second derivative d^2N/dE^2 are indicated by arrows [91K].

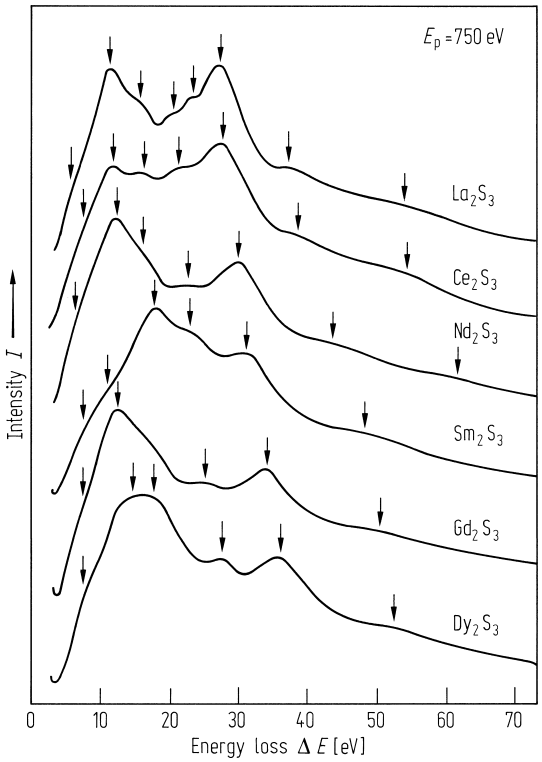

Fig. 28.

γ-Ln_2S_3, Ln = La, Nd, Gd. 4f-4f giant resonance in energy loss spectra at primary electron energy E_p = 750 eV after Shirley background subtraction [91K].

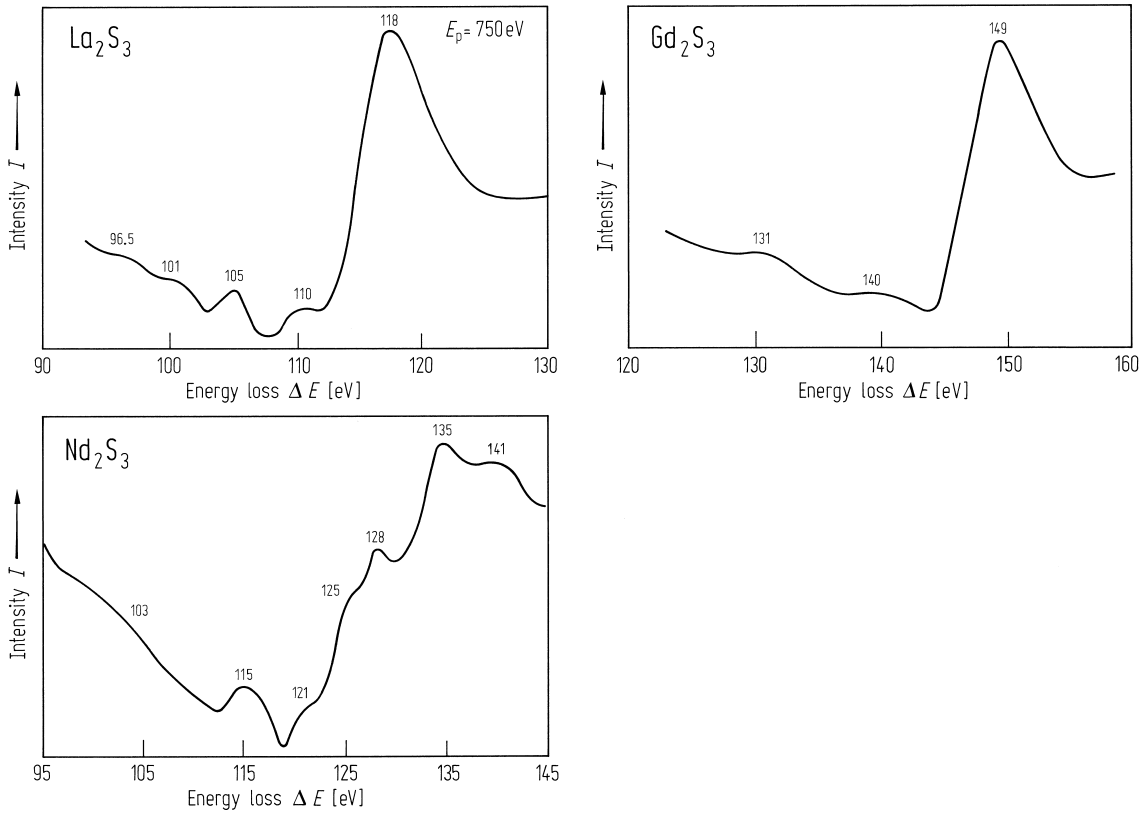

Fig. 29.

γ-La_2S_3; γ-Sm_2S_3. Reflection spectra [83B].